Drone Systems and Applications

OPEN ACCESS | Research Article

Performance characterization of a small portable uncrewed surface vessel for bathymetry mapping near bridges using a single-beam echosounder

Alex Nikonowicz and Artur Wolek

Department of Mechanical Engineering and Engineering Science, The University of North Carolina at Charlotte, 9201 University City Blvd., Charlotte, North Carolina 28223, USA

Corresponding author: **Artur Wolek** (email: awolek@charlotte.edu)

Drone Syst. Appl. Downloaded from cdnsciencepub.com by UNIV OF NC - CHARLOTTE on 03/18/26

Abstract

The performance of a commercially available uncrewed surface vessel (USV) was evaluated through extensive testing in several lakes and rivers around Charlotte, North Carolina, USA, to assess suitability of the platform to be used by a state transportation agency in various bathymetric mapping applications, including collection of sounding measurements near bridges. A first-person-view camera system was integrated onto the vessel to allow surveying in closer proximity to structures. This article reports on the experience gained in operating the USV, including visualization of results from several representative deployments. Data across 41 h of on-water testing at 10 unique locations is aggregated and analyzed to provide statistics concerning the expected battery consumption, signal quality of the global navigation satellite system receiver with distance from occluding structures, vehicle handling characteristics, and different deployment modes. This article may be useful to transportation agency personnel and other users of USV technology to gain a better understanding of the practical considerations, capabilities, and limitations of a representative small USV with a single-beam echosounder.

Key words: uncrewed surface vessel, bathymetry, echosounder, performance

1. Introduction

Uncrewed surface vessels (USVs) have the potential to provide a robust, automated, and cost-effective means to perform tasks such as environmental monitoring, ecological survey, infrastructure inspection, search and rescue, and surveillance (Patterson et al. 2022). While many USVs operate in the ocean and other coastal water, there are numerous industries that utilize USVs in smaller inland water bodies such as ponds, lakes, and rivers. USVs are well suited to perform hazardous tasks, such as surveying mine tailing ponds (Johnson et al. 2016), hard-to-reach areas like construction borrow pits for volume assessment, or small storm-water ponds. USVs can also be used to map bathymetry in rivers and lakes for floor risk assessment (Li et al. 2021), bridge scour monitoring (Schroeder et al. 2019; Kumar et al. 2025), or water quality sampling (Lee et al. 2023; Katsouras et al. 2024). This article reports on the performance characterization of a commercially available USV, the HyDrone USV (Seafloor Systems, Inc. 2025), based on extensive testing in several lakes and rivers around Charlotte, North Carolina, USA. The aim of the testing was to assess the suitability of the platform to be used by a state transportation agency in various bathymetric mapping applications. While there are many existing works that focus on various specific aspects of USV deployment—such as challenges related to global navigation satellite system (GNSS) positioning near structures (Makar 2022; Carilli et al. 2024; Ng et al. 2024), the issue of determining adequate line spacing during bathymetric surveys (Arseni et al. 2019; Adediran et al. 2025), or characterizing USV handling and navigation performance (Marchel et al. 2020; Specht et al. 2019)—they do not focus on providing a practitioner's view of operating a USV for inland environments and bathymetry mapping near bridges. This work aims to fill this gap by presenting a comprehensive overview of operating a specific USV over multiple deployments near bridges and characterizes the aforementioned factors (GNSS availability, line spacing, performance) alongside other practical considerations such as echosounder tuning, recommendations for various deployment modes, and required logistics. The relationship of this article to prior work is further detailed in the following.

While there are many advantages of using USVs, there are also limitations that prevent their use in certain scenarios. Measuring bathymetry near structures is challenging since structures can occlude satellites and degrade the accuracy of GNSS positioning. For example, Carilli et al. (2024) report on the challenges associated with measuring bathymetry under piers and present a solution to operate in this GNSS-denied environment, aided by an ultrashort baseline acoustic positioning system. Ng et al. (2024) also describe the difficulties of operating in a limited space and densely packed bridge

Drone Syst. Appl. Downloaded from cdnsciencepub.com by UNIV OF NC - CHARLOTTE on 03/18/26

pilings and develop a coverage path planner to avoid collision risk with static obstacles. Makar (2022) conducted similar studies that consider both continuity of geospatial data (due to GNSS dropout) and USV navigation safety (due to collision risk). In this article, the effect of GNSS degradation under various bridges is illustrated in experimental data, and a model is developed to represent the observations. Such models can potentially be used in simulation studies or as decision aids to inform the feasibility of collecting data in specific scenarios.

A common sensor employed by USVs to create bathymetry maps is the single-beam echo-sounder (SBES) that measures the depth directly below the vehicle. A SBES reports a single value representing the area ensonified by the SBES footprint on the water body bottom (dependent on the beam width and depth). Multi-beam echosounder (MBES) surveys typically aim to have a specific overlap rate, ensuring complete coverage of an area with a point-cloud dataset, whereas SBES surveys are sparsely spaced without overlap. Both SBES and MBES surveys are conducted with a boustrophedon pattern, where the line spacing is a key parameter controlling the degree of overlap or sparsity. With SBES data, spatial interpolation techniques are used to determine the depth in unsampled regions. Arseni et al. (2019) evaluated different interpolation methods such as simple kriging, radial basis functions, and inverse distance weighting from a SBES in river data. Adediran et al. (2025) studied different interpolation methods and the effect of survey line spacing ranging from 16 to 512 m when interpolating in large 10 km by 10 km areas through simulation studies. In this work, we present an empirical comparison of spatial interpolation accuracy for smaller-scale surveys through a series of field experiments with varying swath width, ranging from 5 to 100 ft, from which a recommended coverage rate is suggested.

Other factors that can affect the accuracy, robustness, and safety of bathymetric surveys include the path following control capabilities of the USV. Large excursions from a desired path can lead to risk of collision, and changes in pitch/roll and heave must be accounted for in correcting bathymetry. Close adherence to planned survey lines is also important for repeatable surveys that revisit the same location periodically. Some researchers have focused on characterizing the control performance of USVs. For example, Marchel et al. (2020) studied the path following performance of an OceanAlpha USV SL20 using a high-precision GNSS RTK, and Specht et al. (2019) characterized the capabilities of a HyDrone that was retrofitted with their own autopilot system and a low-cost GNSS. This work reports performance metrics aggregated over multiple trials for the HyDrone with the vendor-supplied autopilot (AutoNAV Plus).

In summary, the contribution of this paper is the characterization of the performance of the HyDrone through the analysis of experimental data collected over a 2-year period to determine: (i) the degree to which vegetation and buildings impact the available number of satellites to a GNSS receiver, (ii) the effect of changing swathing width in a typical boustrophedon survey pattern on the accuracy of spatially interpolated bathymetric data, (iii) an analysis of the steering accuracy as measured by cross-track error and typical roll/pitch deviations, and (iv) a synthesis of different deployment modes and assessment of their suitability based on various survey factors. Other aspects of working with the HyDrone are reported, including the typical time required to deploy and demobilize the vessel, endurance, and tuning of the echosounder.

Fig. 1. HyDrone deployment in the Catawba River near Charlotte, NC.

2. Hydrone overview

The HyDrone is a small catamaran-style, human-portable USV developed by Seafloor Systems Inc. (Shingle Springs, California) that is widely used for hydrographic surveys (see Fig. 1). For example, the HyDrone has been deployed to investigate landmark-aided navigation approaches using side-scan sonar (Davenport et al. 2025), collect 3D point clouds of the riverbanks using LiDAR and cameras (Sardemann et al. 2023), monitor estuarine shoreline change (Allen et al. 2023), map retention reservoirs (Mach and Skrzypek 2022), and collect bathymetric data in yacht ports (Specht et al. 2020). The system weighs about 25 lbs and is 3.8 ft long making it easy to transport and deploy with a one- or two-person team. The typical survey speed is 2 kts and the platform uses two four-cell 16 000 mAh lithium polymer batteries (nominally 14.8 V). The HyDrone is representative of other USVs of similar size and instrumentation, which commonly include single-beam echosounders (SBESs) for mapping bathymetry.

The HyDrone unit includes a Windows 11 computer called the AutoNav Plus (ANP) with an Intel® Core i3-7100 U CPU, 8GB RAM, and 120GB storage. The ANP enables features such as autonomous waypoint following via Mavlink (a communication protocol) and runs HYPACK software to plan/manage bathymetric surveys and perform analysis.

2.1. Modifications made: custom first-person-view camera system

A custom first-person-view (FPV) camera system was developed to enable teleoperation of the HyDrone. An enclosure was fabricated with a battery power supply, cooling fans, and DJI 03 Air Unit transmitter. The housing was 3D printed and mounted onto the sensor survey pole that provides a view of both left and right pontoons and clear visibility of the region in front of the HyDrone, as shown in Fig. 2. The operator on shore uses FPV goggles to see the water and surrounding

Fig. 2. Operator with first-person-view (FPV) goggles (left), custom DJI Air Unit housing on the HyDrone sensor pole (middle), and view from FPV unit (right).

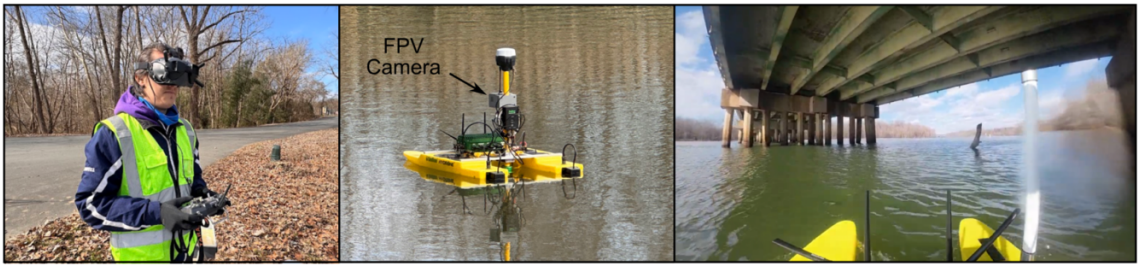

Fig. 3. Sloan's Ferry Bridge testing location consisting of 16 bridge bents.

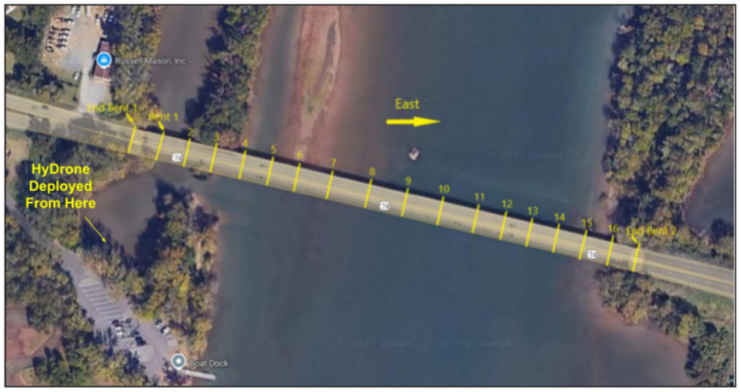

area from the HyDrone's perspective, and this allows identification of hazards that are difficult to observe from a distance.

2.2. Example deployment: Sloan's Ferry Bridge

To illustrate our experience with the HyDrone, this section describes an example deployment of the system near Sloan's Ferry Bridge (latitude: 35.245739, longitude: −81.009163) on the boundary of Gaston County and Mecklenburg County on 24 January 2025. Three sets of data were collected for comparison:

1. Depth measurements using the HyDrone USV in manual (human-operated) mode that allowed close navigation around bridge bents and avoiding very shallow water and large fallen trees near the bridge. Sections of the upstream and downstream parts of the bridge were measured.
2. Depth measurements using the HyDrone USV in automated survey mode. This survey was conducted further away from the bridge in deeper water and on the downstream side following a lawnmower-type pattern.
3. Measurements made by the team using a plumb line from an inflatable raft near each bent on one side of the bridge.

The total time on site for setup, measurements, and recovery, and pack up was approximately 4 h. The GNSS measurements from the HyDrone used corrections from the NC Continuously Operating Reference Station Network with an Emlid GNSS Base and Rover arrangement that received corrections over the internet (using NTRIP protocol) via a mobile phone hotspot. In addition to the above measurements, the GNSS position and altitude of the waterline and the wing wall was recorded. The particular wing wall location was used as a reference point in prior reports studying the bathymetry under this bridge by the North Carolina Department of Transportation (NCDOT) and allowed for comparison to historical data. The testing location is shown in Fig. 3.

During the manual survey (green markers in Fig. 4), an attempt was made to encircle each bridge bent. The operator

Fig. 4. Two data collection runs were executed using the HyDrone uncrewed surface vessel. The first run (green markers) consisted of a remotely piloted survey in the vicinity of the bridge and an outline of a "box" in which to conduct the second automated survey (orange markers).

Drone Syst. Appl. Downloaded from cdnsciencepub.com by UNIV OF NC - CHARLOTTE on 03/18/26

Fig. 5. Depth measurements recorded by the HyDrone uncrewed surface vessel.

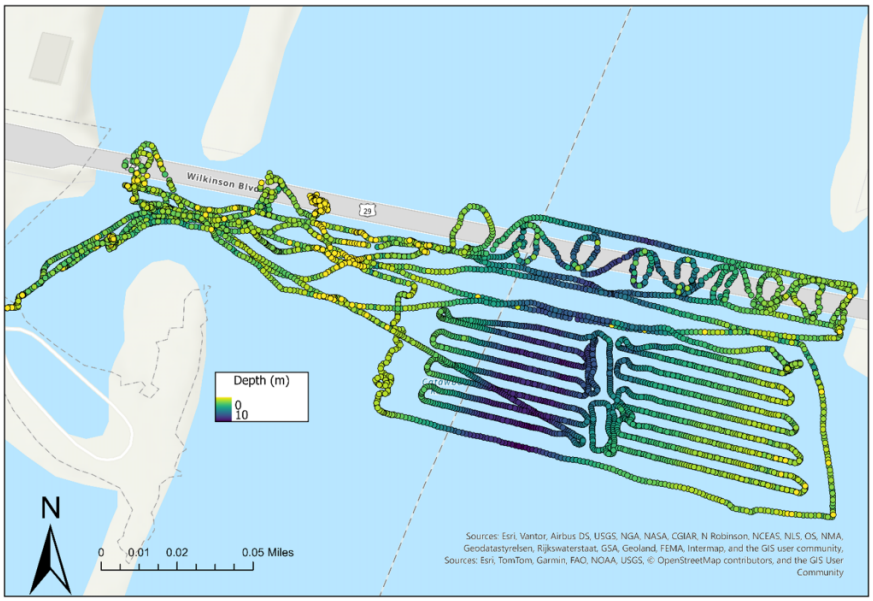

Fig. 6. Depth measurements interpolated and smoothed.

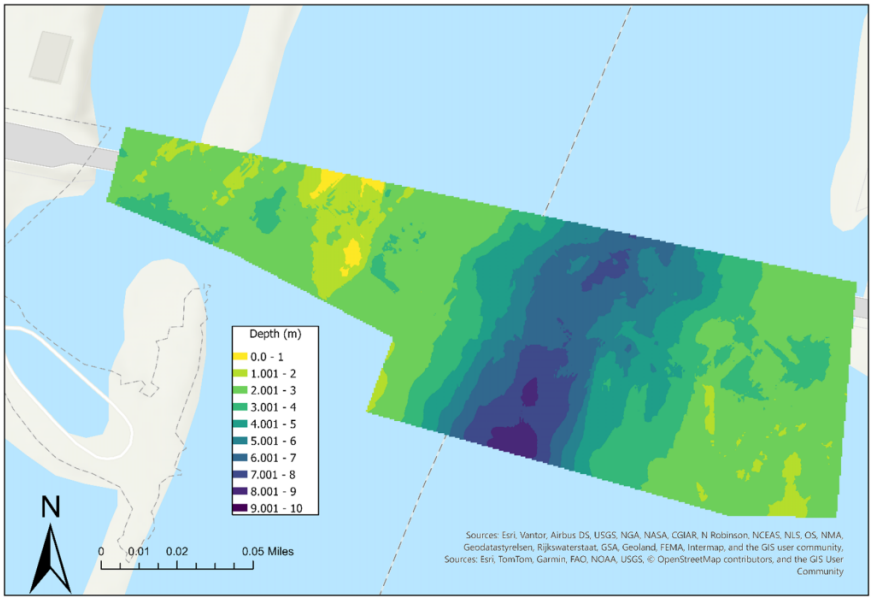

had a live video feed into FPV goggles from the camera onboard the HyDrone. Due to shallow water and debris (trees), some bents were not encircled. A long track alongside the bridge was followed to approximate the location where prior measurements were made from the bridge railing.

The raw soundings of the HyDrone were collected (measured from transducer to river bottom), as shown in Fig. 5. The precision of the sounder measurement is four decimal places in units of m.

The raw measurements were processed to remove a small number of outliers and to add the offset of the waterline to the transducer. Outliers were identified as those values that greatly exceeded the assumed maximum depth of the survey (10 m) by a factor of two or more. Other sources of error may include the assumed speed of sound. Figure 5 results are shown for the low-frequency data (30 kHz). The raw measurements were geostatistically processed using ArcGIS to produce the interpolation in Fig. 6. Standard co-kriging interpolation was used, and the area of interpolation was limited to the region containing measured points and around the bridge area of interest.

To collect additional data for comparison, Bents 1–16 (see Fig. 3) were visited using a small inflatable raft with a trolling motor. A plumb line (an oil-gauging Derrick tape) was used to measure water depth on the downstream side of the bridge, approximately in the middle of each bent. Due to wind and

Drone Syst. Appl. Downloaded from cdnsciencepub.com by UNIV OF NC - CHARLOTTE on 03/18/26

Fig. 7. HyDrone path parallel to bridge and other key points used to rotate the path into the same coordinate system as the streambed profile measurements.

Fig. 8. Comparison of soundings at 30 kHz (left) and 250 kHz (right).

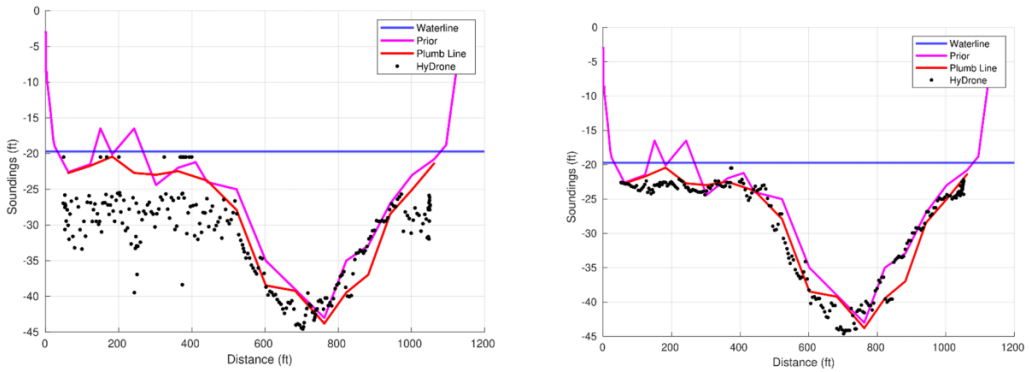

small currents, the inflatable raft was difficult to keep stationary for long periods. Some inherent measurement errors include sag and an angle between the contact point on the riverbed and the tape on the surface. Wave action also introduced errors in this manual measurement. The accuracy of the measurements is likely depth dependent with larger errors for greater depths. The origin point (i.e., the wing wall described earlier) was used to plot streambed profile measurements shown below in Fig. 7. This point was measured using real-time kinematic (RTK) GNSS to be located at (35.24610042, −81.01114885) with an altitude (relative to GNSS reference ellipsoid) of 147.553 m. The waterline near the testing location (−81.01148520, 35.24554618) was measured with RTK GNSS to be at an altitude of 141.543 m. Therefore, we assume the waterline was about 6.01 m (19.71 ft) below the origin point during the day of the test. The streambed profile has the abscissa defined parallel to the bridge. To properly align and rotate the HyDrone measurements to be consistent with this direction, two points along the bridge centerline were selected based on satellite imagery (see below). From these points the orientation of the bridge was found to be −13.469 deg. South of East.

Figure 8 compares the prior NCDOT measurements (obtained on 23 February 2024) to the plumb line measurements and the low-frequency (33 kHz) HyDrone measurements (limited to the first line of the test that was parallel to the bridge). Both the plumb line and HyDrone measurements are plotted by offsetting them from the origin by the amount determined as the waterline (19.71 ft) above. The plumb line measurements appear to be similar to the prior NCDOT measurements with the deepest point of the channel occurring at about 760 ft near Bent 11. The HyDrone was deployed parallel to the bridge but offset by about 12 ft during this manually piloted run. Measurements near the deepest point of the channel are similar, although they are shifted to the left with the deepest point at about 700 ft. This appears to be consistent with Fig. 4 that shows the overall geometry of the channel skewing toward the center of the river downstream of the bridge. The HyDrone measurements exhibited low noise when operating in deeper water. However, high noise and unreliable measurements were observed in the shallow sections of the river that had a depth of less than 5 ft (at distances between 0 and 500 ft seen in Fig. 8 and later on the east bank of the river near distances of 1000 ft). The HyDrone transducer was mounted 0.77 ft below the waterline and at depths of a few feet is susceptible to reverberations and other acoustic and signal-processing limitations. When comparing the high-frequency (250 kHz) HyDrone measurements, a much better consistency and agreement with prior data and plumb-line measurements were observed.

Drone Syst. Appl. Downloaded from cdnsciencepub.com by UNIV OF NC - CHARLOTTE on 03/18/26

Fig. 9. Global navigation satellite system (GNSS) data from a survey on Hechenbleikner Lake, NC. Left: path of uncrewed surface vessel color-coded by percentage of satellites in sky-view of GNSS receiver; right: satellite image of survey area with plots showing where vegetation and buildings are located.

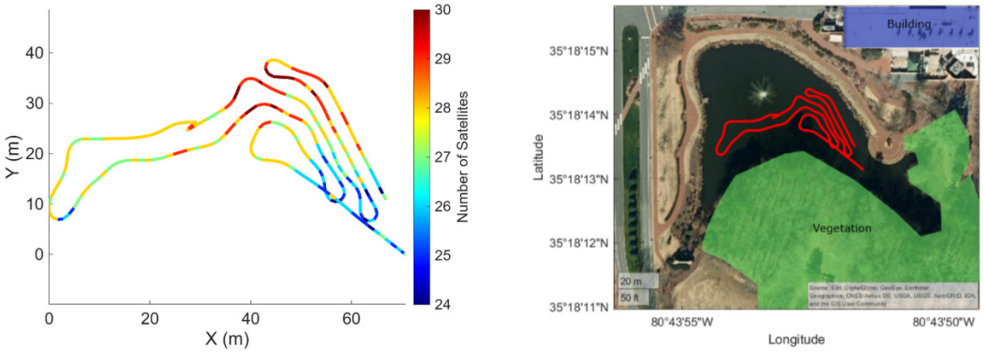

3. Analysis of USV performance over multiple deployments

The HyDrone used in data collection for this research was deployed 25 times at 10 unique locations with a total survey in-water time across all testing being 41 h. Field experiments were designed to assess the viability of different survey modes, to collect bathymetric results, and to evaluate vehicle performance and echosounder tuning procedures. The experiments described in the following sections were completed to provide evidence of proper USV deployment practices and draw conclusions about using a USV for rapid inland bathymetry assessment.

3.1. Effect of vegetation and infrastructure on GNSS data quality

The GNSS data are a critical part of the HyDrone's operation. It is used in geostatistical processing when interpreting bathymetric data and for autonomous waypoint control. Inaccurate GNSS data can cause errors in the measurement locations, leading to inaccurate bathymetry, or may cause the vehicle to deviate from its intended path, which can lead to unexpected collisions or running aground. The testing data were analyzed to determine the degree to which GNSS errors affected the HyDrone. The metric used to determine GNSS signal quality in these experiments was the percent of satellites in sky-view. Sky-view, as it relates to a GNSS receiver, refers to the amount of unobstructed space above the receiver to view GNSS satellites. Normalizing the dataset to percent of satellites in sky-view, based on the maximum number of satellites seen during a survey, allows for comparison across datasets and can indicate other quality-based GNSS statistics like dilution of precision (DOP). When performing hydrographic surveys with a USV, two main sources of sky-view obstructions are vegetation and infrastructure. Vegetation includes tall trees surrounding the survey region, and infrastructure includes bridges and buildings. The environment can also impose an obstruction due to steep banks or various terrain profiles. Consider the data from a survey at Hechenbleikner Lake, NC, shown in Fig. 9, that was conducted in the presence of a building and vegetation.

The maximum number of satellites viewed in this survey was 30, and the minimum was 24. Vegetation on the south side of the lake obstructed the sky-view by about 20% of the viewable satellites, although a high number of satellites remained visible, and the GNSS position estimate was not greatly affected. The building present on the northeast side of the survey area was too short and distant from the survey area to have any significant effect. For comparison, the trees are estimated to stand at about 25 m tall while the building is about 12 m tall. When vegetation obstructs sky-view, factors such as tree density, tree height, and distance of the USV from the vegetation will play a significant role in the severity of the GNSS degradation.

Figure 10 shows GNSS satellite view data from a survey at Mountain Island Lake, NC. This survey had dense tree coverage around the inlet survey region with trees about 27 m tall. While GNSS degradation is seen on the south side of the survey and within the eastern part of the inlet, a sufficient number of satellites are in view of the receiver to produce accurate GNSS data (the number of satellites ranged from 25 to 31). Dense tree coverage can restrict the receivers sky-view but did not appear to have a major effect on receiving high quality GNSS data, given the distance of the USV from shore. As evidence of this, Fig. 11 shows the DOP and GPS mode data from the Mountain Island Lake survey.

The percentage of satellites viewed decreases across points at the beginning of the survey and consistently at the end of the survey, indicating satellites moved outside the area of the receiver's view at the end of the survey. However, the DOP only increases by 0.1 for the duration of the survey. GNSS data DOP values below 1 are considered very accurate. The GNSS mode for the entire survey remained at 4, indicating the GNSS data are receiving its corrections and no drop-out occurred.

Bridges spanning the region of interest have more of a direct impact on the receiver's sky-view, as the receiver has to survey adjacent to, or directly under, the bridge. Several surveys were conducted in bridge environments; the following survey analysis (see Fig. 12) was conducted in the Catawba River in Gastonia, NC (corresponding to the case study presented earlier).

Drone Syst. Appl. Downloaded from cdnsciencepub.com by UNIV OF NC - CHARLOTTE on 03/18/26

Fig. 10. Test #12 global navigation satellite system (GNSS) data. Left: Mountain Island Lake, NC survey showing satellites in sky-view of GNSS receiver. Right: Satellite image of survey area with plots showing where vegetation locations.

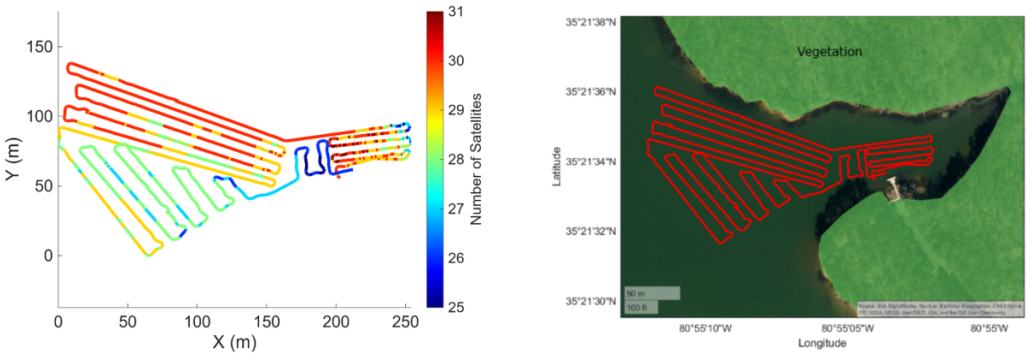

Fig. 11. Global navigation satellite system (GNSS) data quality statistics for Mountain Island Lake, NC survey.

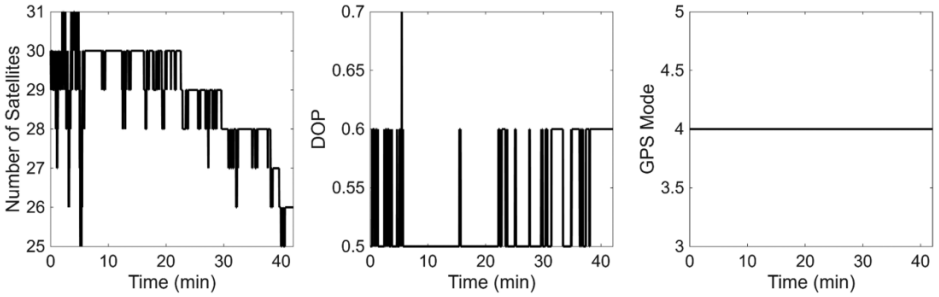

Fig. 12. Test #22 global navigation satellite system (GNSS) data. Left: Catawba River bridge survey showing satellites in sky-view of GNSS receiver. Right: Satellite image of survey area with plots showing bridge and vegetation locations.

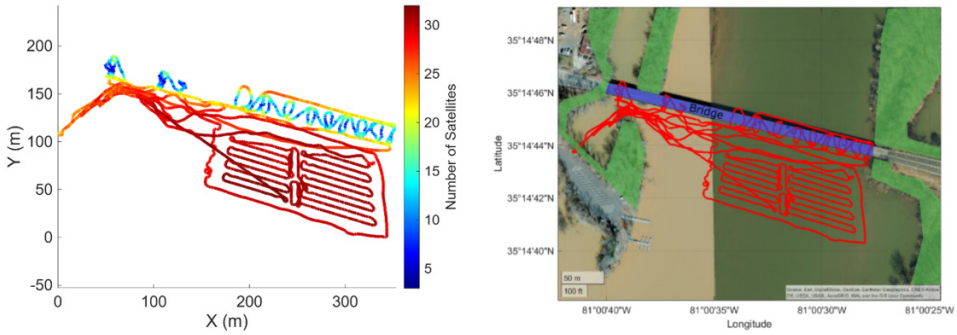

Figure 12 shows the satellite percentage data for the entirety of the bridge inspection, where satellite loss is more dominated in this area when compared to surrounding vegetation. In most areas under the bridge, satellites in sky-view drop to 10%–30% from what was visible in the open areas. The dimensions of the bridge are about 12 m wide and 6 m above the water level. In this survey, a maximum of 32 satellites were in the view of the receiver with a minimum of 3. While there are filters and estimation techniques that can mitigate the effects of intermittent signal loss, long periods of time under this type of bridge environment are not sustainable. Figure 13 shows the standard deviation of horizontal position error from sensor data being recorded under the bridge.

Fig. 13. Horizontal position error from the data that was recorded under the bridge.

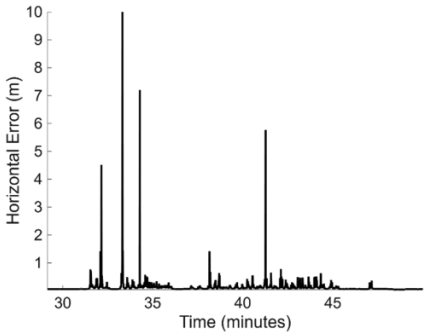

Drone Syst. Appl. Downloaded from cdnsciencepub.com by UNIV OF NC - CHARLOTTE on 03/18/26

Fig. 14. Percent of satellites in sky-view based on absolute distance from the center of the bridge. Left: Test #17 (Bridge 1), middle: Test #21 (Bridge 2), and right: Test #22 (Bridge 3).

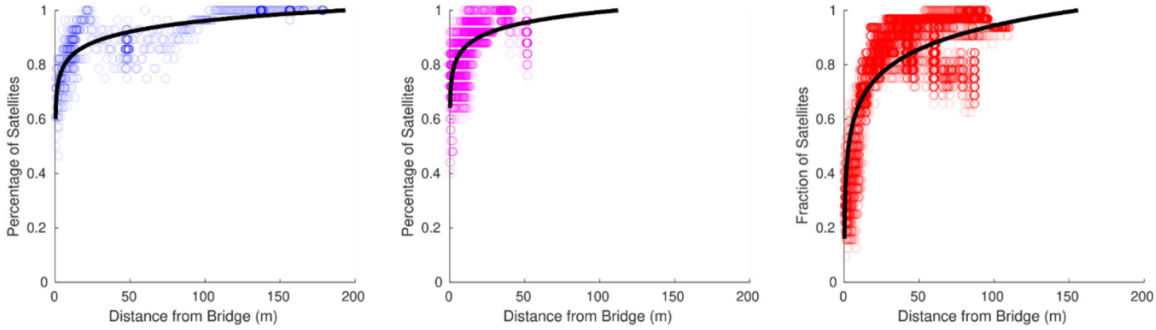

Drone Syst. Appl. Downloaded from cdnsciencepub.com by UNIV OF NC - CHARLOTTE on 03/18/26

At some instances, the horizontal error can be as high as 10 m due to the low number of satellites the receiver has to compute its position. While under the bridge, most of the horizontal error measurements are around 0.7 m, and the error returns to near-zero value after the USV egresses from under the bridge.

To visualize the effects that bridges have on GNSS data quality, three bridge surveys are compared with different physical measurements to show the severity of satellite loss. The Gastonia bridge data (Test #22; bridge with height of approximately 6 m and width of 12 m) are compared to data collected from Cowans Ford, NC (Test #21; bridge with height of approximately 11 m and width of 8.5 m) and Mountain Island Lake, NC (Test #17; bridge with height of approximately 15 m and width of 8 m) bridge locations.

Figure 14 shows the satellites in sky-view with a logarithmic curve fit to the data based on the absolute distance from the center of the bridge.

The curve fits had R^2 values of 0.672, 0.457, and 0.537, respectively. The fit models were

$$\text{Bridge 1}: \; p = (0.1340)\log(h) + 0.6936$$
$$\text{Bridge 2}: \; p = (0.1307)\log(h) + 0.7321$$
$$\text{Bridge 3}: \; p = (0.2908)\log(h) + 0.3625$$

This model should be clamped between a value of zero and one. Using the satellites in sky-view data from these three tests, it can be determined that the physical properties of a bridge have a great impact on the accuracy of GNSS data. In Tests #17 and #21, the data had about a 30% loss of satellites in sky-view while under the bridge, and high-accuracy position data were still maintained. This contrasts the data from Test #22, which saw an 80% reduction in viewable satellites and had large variation estimates for the recorded positional data. The R^2 values obtained indicate that the distance from the bridge centerline has a moderate ability to explain or predict the changes in percentage of satellites. However, there is still considerable variability in the percentage of satellites, even for similar distances. This variability may be attributed to factors such as random errors that occur when processing GNSS signals, changes in true satellite availability over the duration of the USV's deployment, and potential GNSS multipath issues that may arise and vary along the length of the bridge. Additionally, the presented models are reported for bridges of various widths and height; however, caution should be used when applying the results to different bridges. Bridge material and construction style may also affect GNSS signal attenuation.

3.2. Effect of swathing width on bathymetric data accuracy

Using SBES technology to collect and analyze depth data requires the USV to survey a region in a way that considers how geospatial interpolation will later be conducted. Because the SBES measures one depth value for every position point, densely sampling the environment to create a high-resolution raster map of the seabed is unrealistic. Geostatistical processes like kriging are used instead to interpolate in unsampled regions. Boustrophedon (i.e., "lawnmower" style) paths are commonly used to uniformly sample the environment and can be planned with different swathing widths, also referred to as line spacings. To determine the percentage of area covered with a particular swath width, the echosounder footprint is estimated for each data point, and the resulting depth is determined based on the average amplitude of the returning sounding measurements.

An experiment was designed wherein the HyDrone operated autonomously in a predefined area at different swathing widths (100, 50, 33, 20, 10, and 5 ft), leading to coverage paths of 2, 3, 4, 6, 11, and 21 lines, respectively. The accuracy of geostatistical analysis was characterized as a function of the area covered by the echosounder footprint. The results are shown in Figs. 15 and 16. Note that some spurious measurements are visible but were not removed to leave the dataset unaltered.

In each of the surveys, the total seabed area that each echosounder footprint observed is summed to quantify the total area covered. The coverage is calculated according to $A = N\,\pi\,r^2$ where N is the number of measurements and $r = \tan(\alpha/2)\,d_{\text{avg}}$ is the footprint radius considering the average depth in the environment (approximately $d_{\text{avg}} = 3.803$ m) and the beam width of the sonar ($\alpha = 6^\circ$ for high frequency data). The coverage area calculation above assumes that the N measurements are non-overlapping, which in this case holds true since $r = 0.1660$ m and the average distance between measurements was 1.378 m. For a more accurate coverage area

Fig. 15. Swath width tests with echosounder data.

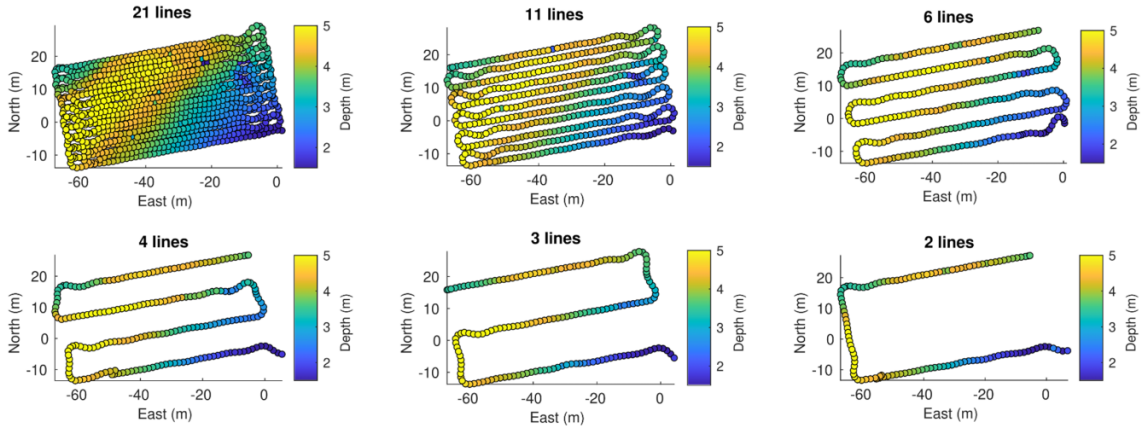

Fig. 16. Spatially interpolated data using ordinary kriging.

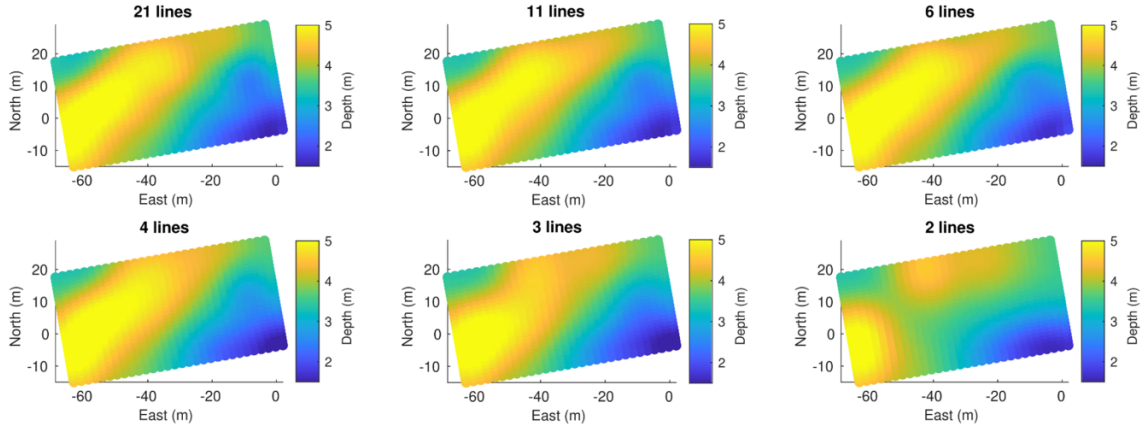

calculation, the average depth can be replaced with a local depth value, but this is not known beforehand. Thus, we use the average depth, which is easier to estimate for planning surveys. The total survey area was the same across all tests.

Each of the krigged models in Fig. 16 were computed in MATLAB using the ordinary kriging algorithm. This interpolation method requires defining a kernel, which was selected as the squared exponential kernel:

$$k(h) = \sigma^2 \left(\frac{h^2}{L^2} \right)$$

where $L = 20$ m, $\sigma^2 = 5$ m. The interpolation was performed over a grid of 30^2 points with length of 66 by 33 m rotated to approximately overlap the survey region.

As expected, more swaths led to a finer level of detail shown in the raster plots. The results for the 2- and 3-lines plots in Fig. 16 are substantially different from highest resolution plot with 21 lines. The results for 4-, 6-, and 11-line plots are more consistent. To further evaluate the effects of the different swathing widths, the RMS error was calculated assuming the densest dataset (21 lines) as ground truth. Since no other high resolution bathymetric data set could be identified that covered the survey area, the interpolation with the 21-swath dataset was selected as the ground truth for comparison as it had the largest number of datapoints. All the data was collected with the same echosounder (Hydrolite Plus Dual Frequency) which has a manufacturer-stated accuracy of 1 cm or 0.1% of depth measured. Any systematic bias (e.g., due to sensor calibration and settings) equally affected all datasets. In Fig. 17, the relative error as a function of echosounder area coverage shows diminishing returns in data accuracy with survey line density. The two-line path had an average error of 4 ft depth and the 11 line path had an average error of 0.5 ft with an exponential trend in-between. This is expected as overall accuracy will increase with data density. This experiment shows that the RMS error is around 0.5 ft when using 3% area coverage.

From this analysis, we recommend that swaths should be placed such that at least 3%–5% of the total survey area will be covered with soundings when operating on length scales similar to those tested. Of course, other regions that exhibit greater variability may require even higher coverage rates.

3.3. Characterization of cross-track error and pitch/roll deviations

Cross-track error refers to the lateral deviation of a vessel from its planned path and impacts vessel safety and data accuracy. When operating the vessel in its autonomous mode, the surveyor should understand how accurately the waypoint

Drone Syst. Appl. Downloaded from cdnsciencepub.com by UNIV OF NC - CHARLOTTE on 03/18/26

Fig. 17. Relative RMS error of each of the swath test where the 20 swath test was used as the baseline.

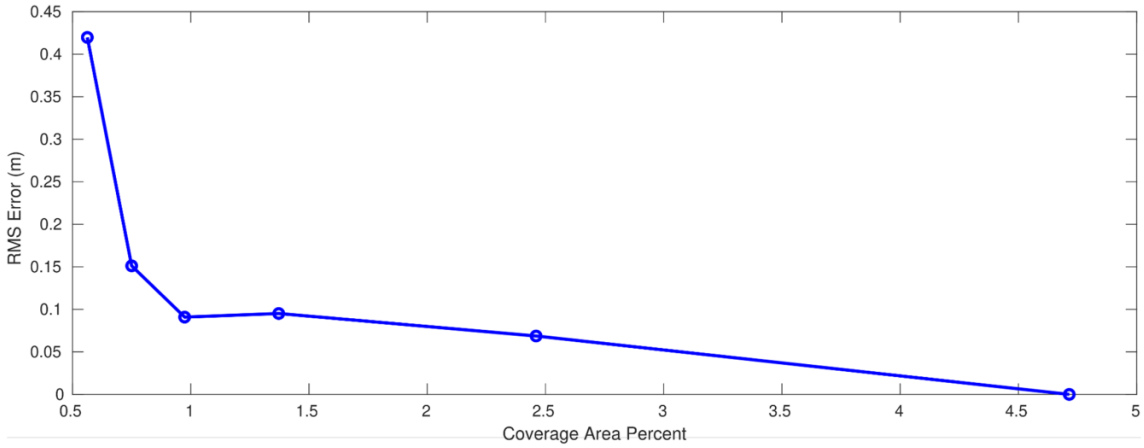

Fig. 18. Cross-track error data from experiments in Mountain Island Lake, NC.

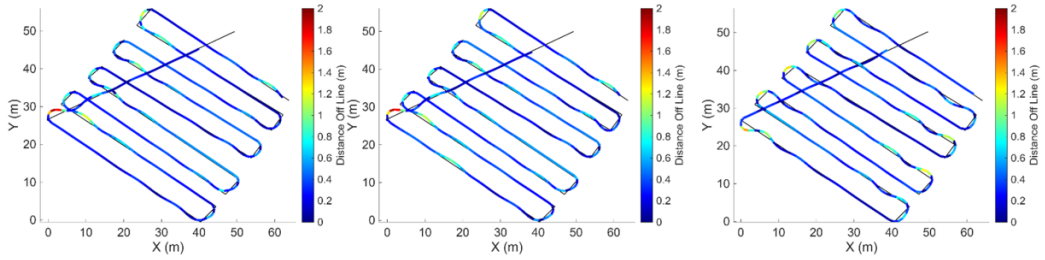

Fig. 19. Cross-track error data from Test #12 in Mountain Island Lake, NC (left: cross-track error with time, right: cross-track error overlayed on path).

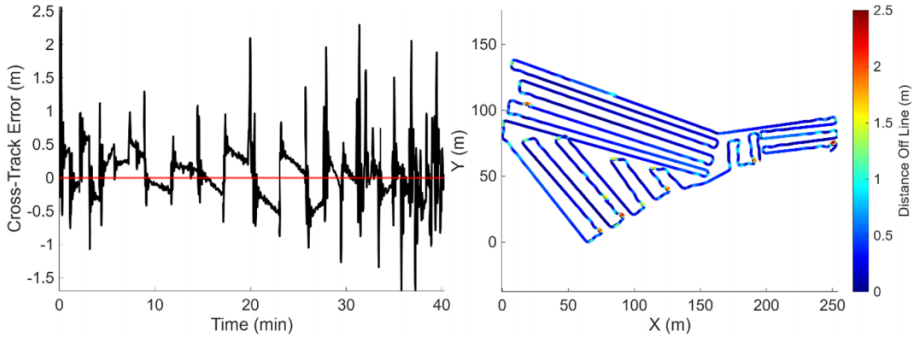

path is traversed. Excessive overshoot, along with poorly placed waypoints, may cause vessel damage due to collision with in-water obstacles or it may result in missing the intended measurements. While performing autonomous surveys with the HyDrone, cross-track error was measured in different scenarios.

In this first analysis, cross-track error is visualized on three similar surveys (see Fig. 18). Each survey used the same waypoint path to evaluate consistency. The cross-track error is plotted on the GNSS trace from the recorded survey to analyze where cross-track error occurs and its severity.

Analyzing the results of the cross-track error data in the autonomously controlled survey, the vessel tends to stay within 0.3 m of the planned path waypoint path on straight sections. During turns, the vessel exhibits more variability in the amplitude of cross-track error before returning to its straight-line behavior. Large deviations consistently occur at the turning points, albeit with varying amplitudes near about 1 m. To return to its straight-line behavior, the vessel motion oscillates on the waypoint path to correct for its overshoot. The results show that the path of the USV is relatively consistent across the three trials, although there are some exceptions, such as the oscillations apparent in the second and third tests on the outermost line are missing from the first test. This example used a standard boustrophedon path with little variability in the turning angles. Cross-track error data from another test with more unique turning angles is shown in Fig. 19.

Drone Syst. Appl. Downloaded from cdnsciencepub.com by UNIV OF NC - CHARLOTTE on 03/18/26

Fig. 20. Cross-track error plotted by density across several HyDrone tests.

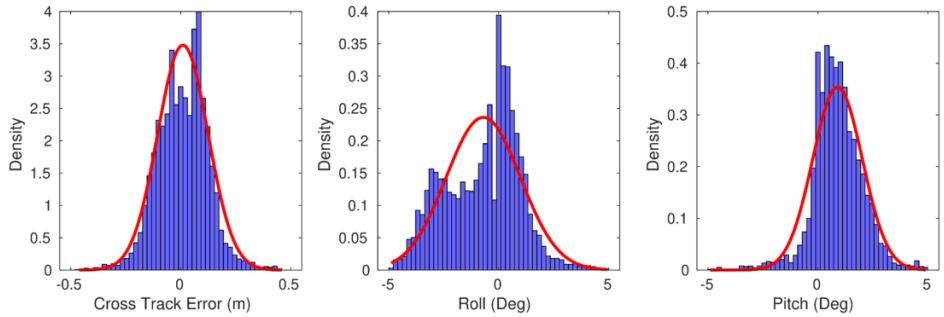

Fig. 21. Battery drain percentage plotted against in water survey duration.

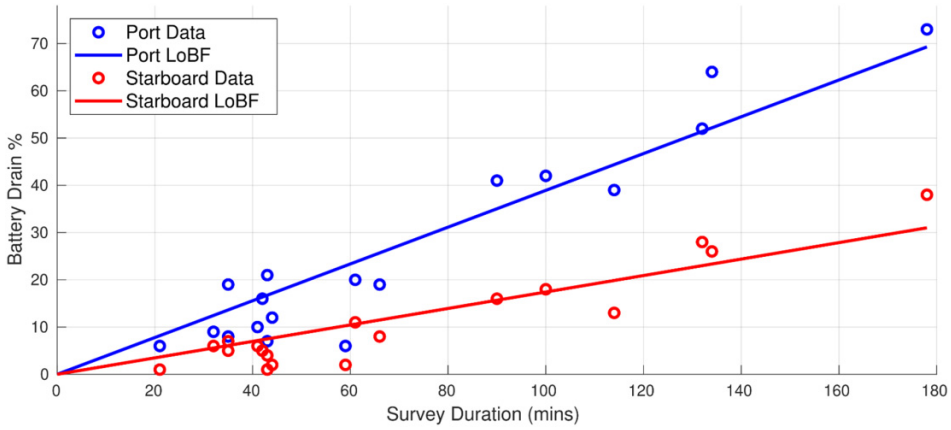

Due to the size of the survey area, the large cross-track error, colored in red, is mostly absent; however, during tight turns, light blue and green colors appear denoting that large cross-track error occurred before decaying. The plot of cross-track error versus time shows the large spikes in path deviation before quickly returning to the straight-line variance. For the first half of the survey, right-angle turns are taken, and the maximum amplitude in these areas is around 1 m of error. In the later half, tighter turns are taken, and greater cross-track error is observed in comparison to slight turns. In the middle of the time plot, after a turn indicated by a large spike in cross-track error, the cross-track error does not return to zero. In some cases, the error trends away from zero at a constant rate. While the magnitude of error is still small, it indicates that the onboard control system tolerates a deadzone of heading and/or cross-track error. For the vessel to successfully "visit" a waypoint, it must be within 2 m of the target waypoint. The straight-line error is almost six times smaller than this requirement, and this small cross-track error does not impede the vessels waypoint-following ability.

Figure 20 shows a histogram of recorded cross-track error, roll angle, and pitch angle across eight tests (multiple days of autonomous survey) representing 152 min of data.

A Gaussian distribution was fit to each dataset to give values of mean (μ) and standard deviation (σ) of (μ, σ) = (0.0096 m, 0.1146 m) for cross-track error, (μ, σ) = (-0.704°, 1.689°) for roll, and (μ, σ) = (0.890°, 1.128°) for pitch. The results indicate that the HyDrone can follow survey lines with a high degree of accuracy, and roll and pitch deviations are relatively small. The results were obtained under nominal conditions without significant water currents or waves.

3.4. Characterization of USV deployment and recovery logistics

To make conclusions about the ease and required time for personnel to operate the HyDrone, the total survey time, battery drainage, and deployment time were recorded across all the experiments. The goal of providing these data points is to give a surveyor who is unfamiliar with a USV-integrated bathymetric survey an idea about the time commitment, limiting factors, and typical survey requirements. The mean setup time was 27.7 min (11.1 min standard deviation), and the mean pack-up time was 29.4 min (12.9 min standard deviation).

Throughout testing, the same starboard- and port-side batteries have been used in their respective housings. This is done so we can analyze the performance of each battery. We only considered longer tests that drained the port-side battery by more than 5%. Shown in Fig. 21 are the battery drainage percentages plotted against survey time. Looking at the data for the port-side battery, the battery drains faster than the starboard-side battery at almost double the rate, and it causes a bottleneck for total survey endurance.

Drone Syst. Appl. Downloaded from cdnsciencepub.com by UNIV OF NC - CHARLOTTE on 03/18/26

Fig. 22. Test #17 showing the difference in low- and high-frequency data.

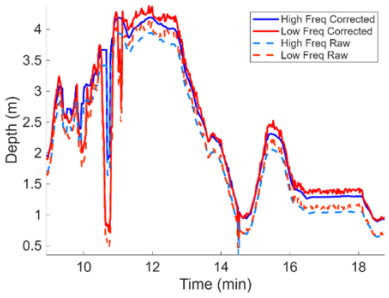

Fig. 23. Test #12 data with significant error in shallow water within the deadzone range.

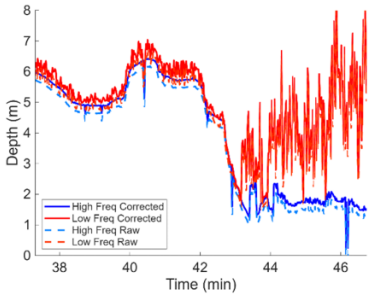

A line of best fit that passes through the origin was drawn through each dataset, leading to a slope of 0.3893 (% battery drain/minute) for the port side and 0.1742 (% battery drain/minute) for the starboard side. Following the line of best fit, the port-side battery limits the total survey time to about 3 h if fully charged.

3.5. Effect of echosounder tuning

The HyDrone is equipped with a Hydrolite Plus SBES, also manufactured by Seafloor Systems. The Hydrolite Plus SBES includes the capability to record georeferenced echogram information for post-processing. Echosounder settings that can be adjusted include maximum range (m), interval between echosounder pings (s), transmit length (microsec), transmit power (dB), receiver gain (dB), time interval (microsec) to attenuate −20 dB, minimum range deadzone (m), threshold (%) minimum amplitude, device position offset (m), and speed of sound (m/s). The SBES unit is pole-mounted and can be removed from the USV to be used on a flat-bottom boat for more conventional manned surveys. Low-frequency data generally are considered to have greater range and can penetrate soft bed types, including sand, mud, and clay. High-frequency data tend to report lower depth values at shorter ranges but with higher resolution and less noise, and do not penetrate the lake bed or riverbed.

Figure 22 shows data from Test #17, where low- and high-frequency data were used to record data from under a bridge in Mountain Island Lake, NC. The raw data are corrected by accounting for the offset of the transducer and the orientation of the vessel. This results in the corrected data being deeper than the raw data, as the transducer is set to around 0.2 m below the surface of the water. When looking at the trends of both high- and low-frequency data, the high-frequency data are about 0.1–0.25 m shallower than the low-frequency data. This may indicate that in those areas of the survey, there is a soft bed type where the thickness of the loose sediment is the difference between the two depth measurements.

The echosounder's gain setting controls the sonar receiver's sensitivity to the measured water columns depth and turbidity. Increasing the gain can provide finer detail in the echogram, which translates to more accurate measurements. However, it may also increase the amount of noise due to water impurities, aquatic life, and bed type changes (e.g., transitions from sand and silt to rocky bottoms). The manufacturer's recommendations for clear water with hard, solid bed types are to use negative gain values, as low amounts of noise should be present and would be considered an ideal scenario for surveying. Positive values of the gain setting are recommended for soft bed types, impure water conditions, and deep-sounding survey scenarios. Range and dead zone settings refer to the maximum and minimum values that the echosounder will output and operate in. These settings are important to tune since, even in ideal conditions, erroneous data may result if they are incorrectly set.

Figure 23 shows data from Test #12 in shallow water. The high-frequency data with a deadzone of 1 m were recorded as expected, while the low-frequency dataset with a dead zone of 2 m showed noisy readings. Because the true depth of the area is around 1–2 m and the deadzone exceeds that at 2 m, the recorded depth for this area became erratic. We have found that deadzone and range tuning is particularly important in shallow environments where correct echosounder output is more sensitive.

Correct echsoounder param can be challenging to predict for an unknown body of water. However, the echosounder can be tuned on-site by running the system iteratively (starting with default settings) over a subset of the survey area and tuning param in-between trials (by observing degree of noise in output depth or comparing to known values). In Test #23 at Lake Norman, NC, multiple tests were conducted using the same waypoint path comparing the default echosounder settings to other tuning configurations (see Fig. 24).

Table 1 shows the settings used in each of the three experiments shown in Fig. 24. The middle datasets show default settings, while the left and right datasets represent semi-tuned and fully tuned echosounder param.

Range, transmit length, and threshold were all tuned based on prior knowledge of the environmental area and on-site observations. Transmit length can be tuned by considering the water quality and bed type, where the threshold can be set based on maximum range assumptions. The interval or sampling frequency was changed from the default 1–5 Hz to increase the amount of data collected in experimentation. Range for both semi and fully tuned tests was decreased to 10, as the maximum depth seen was about 5 m. The main differences between the semi-tuned and fully tuned tests was the gain, which improved performance in Lake Norman's murky waters.

Drone Syst. Appl. Downloaded from cdnsciencepub.com by UNIV OF NC - CHARLOTTE on 03/18/26

Fig. 24. Lake Norman Test #23 echosounder tuning with three test iterations. Left shows poor tuning, middle shows default setting, and right shows good tuning procedures. The top images show depth plotted with global navigation satellite system trace, and bottom shows depth indexed by each data point collected.

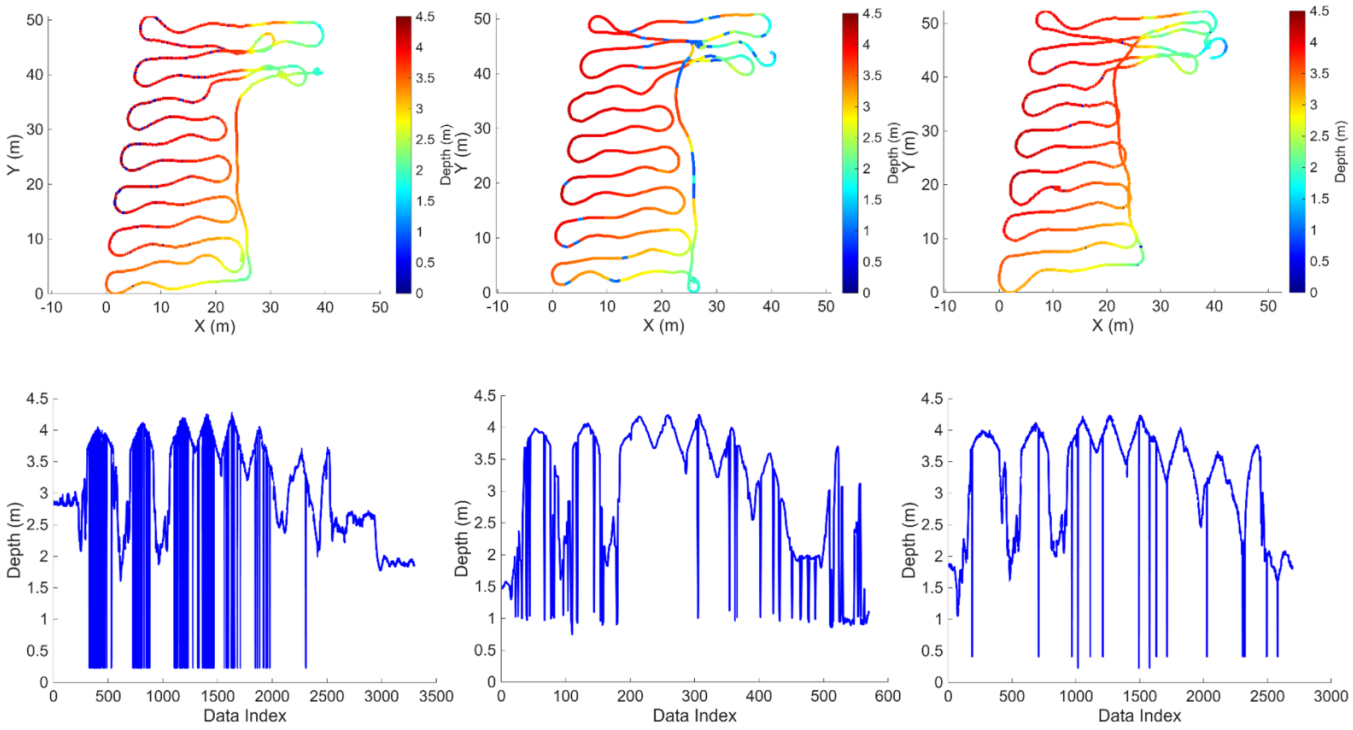

Table 1. Settings used for Test #23.

Setting	Semi-tuned	Default	Fully tuned
Range (m)	10	30	10
Deadzone (m)	0.2	1.5	0.2
Interval (s)	0.2	1.0	0.2
Gain (dB)	0	0	6
Threshold (%)	15	10	20
Transmit length (μs)	15	30	15

4. Deployment methodologies

The HyDrone USV was deployed in several environments and contexts to evaluate different modes of operating the vessel, as summarized in Fig. 25.

Factors that can influence the most appropriate mode include the presence of obstacles or debris, the distance at which the survey will be conducted from shore, the expected area to be covered, the visibility of the HyDrone during the survey, and water current. Table 2 lists the identified deployment modes and the survey factors that may be used to help determine which mode is suitable (indicated by an "X"). Rankings are given from optimal (1) to least optimal (4) for the large area coverage and labor intensity factors of each mode.

The modes are detailed in the following:

4.1. Manual remote control

Remote-controlled surveys are conducted entirely by the operator with the handheld transmitter. When controlling the USV by a transmitter, the USV has more maneuverability in the survey area, which can be useful when surveying in constrained spaces or around vegetation. Due to the human factor in controlling the USV, data density and line spacing may be highly varied throughout the survey region. The vessel may be difficult to accurately control past 200 ft as it becomes difficult to observe and discern its relative position to obstacles and orientation. Remote-controlled surveys are most beneficial in small lakes or ponds where the line-of-sight of the vessel in the survey area can be fully maintained by the operator.

4.2. First-person-view teleoperation

Similarly to a remote-controlled survey, the operator can control the USV from the perspective of the USV. This operational mode uses the FPV camera to provide an "onboard" perspective of the drone to the surveyor. This survey mode enables maneuvering precisely around obstacles at a distance and in cases where the vehicle is temporarily occluded (e.g., when passing behind a bridge pier). The operator loses their peripheral vision of the surrounding when operating in this mode, and it is best to have a second individual serving as a "spotter" while the operator is in FPV mode.

Drone Syst. Appl. Downloaded from cdnsciencepub.com by UNIV OF NC - CHARLOTTE on 03/18/26

Fig. 25. Different approaches for deploying and operating a portable uncrewed surface vessel in survey of inland bodies of water.

Table 2. List of survey modes and factors that influence mode choice.

Survey factors	Manual remote control	FPV tele operation	Autonomous waypoint survey	Boat-deployed hybrid survey	Wading operator	Tethered operator
0–500 ft range	X	X	X		X	X
>500 ft range		X	X	X		
>1000 ft range				X		
Intermittent line-of-sight		X	X	X		
Constrained environment	X	X			X	X
Small region (<1000 sq. ft)	X	X			X	X
Medium region (<10 000 sq. ft)			X	X		
Large region (>10 000 sq. ft)			X	X		
Fast-flowing water						X
Obstacles or debris present	X	X			X	
Long duration survey	4	3	1	1	4	2
Labor intensity	2	2	1	3	4	4

Note: FPV, first-person-view.

4.3. Autonomous waypoint survey

An autonomous survey requires a survey area to be defined either from satellite images or previous surveys so that a reference can be used to place waypoints. The operator then monitors the USV as it autonomously collects bathymetric data. This mode provides a repeatable method of collecting data (e.g., periodically to monitor changes) and is ideal for large, unobstructed environments.

4.4. Boat-deployed hybrid mode

This survey mode involves operating the USV from a manned boat. The USV can either be deployed from the manned vessel or travel alongside the operators from a boat ramp to the survey destination. This approach has the benefit that it allows sampling in areas where there is no convenient launch point (due to inaccessibility, steep walls on a riverbank, etc.) or operating in areas that would be too far due to communication range limitations from shore. The mode can involve both hybrid control of the USV (teleoperation and autonomous waypoint control). Teleoperation from the boat supports steering the USV to the survey location during transit or collecting measurements in challenging environments with obstacles, while autonomous control can be used to survey larger remote areas.

4.5. Wading mode

A surveyor can deploy the USV in a small creek or stream and control it from wading in the stream itself. In difficult-to-traverse terrain with many rocks, shallow regions, and vegetation growing in the water, it may be simpler to operate the drone this way, as it provides better visual perspective of obstacles than standing from shore. This method can be particularly useful in scenarios where measurements are normally

Drone Syst. Appl. Downloaded from cdnsciencepub.com by UNIV OF NC - CHARLOTTE on 03/18/26

taken using depth gauges via wading; the USV enables collecting measurements more efficiently and in areas that are too deep to wade in can be collected. However, there are also limitations, in that the USV has a minimum operating depth and may need to be frequently re-adjusted or carried when traversing over very shallow areas where it is caught on terrain, rocks, or vegetation. The depth should be at least 2 ft to allow the USV to operate reliably.

4.6. Tethered mode

In the case that a stream or river flow exceeds the capabilities of the USV, bathymetric data can still be collected by tethering the USV to a harnessed operator, a bridge, or a fixed point. This tether will act as a pendulum, as the operator controls the USV, moving it from side to side and collecting bathymetric data. The tether is lengthened or shortened to change the distance from the operator and swathing width.

5. Conclusion

This paper reported on the performance and practical aspects of operating a HyDrone USV (representative of a class of similar man-portable USVs) for bathymetric data collection in inland bodies of water. An example deployment in which data were collected near a bridge illustrated the benefits of using a combined survey mode involving both FPV teleoperation and autonomous waypoint planning that favorably compared the echosounder data to other measurements using a simple plumb line. The aggregated data across multiple trials provide insight into the USV's performance and limitations. A logarithmic model was developed to represent the number of satellites available for GNSS positioning with distance from a bridge, illustrating that lower and wider bridges can severely degrade GNSS performance. Field experimentation that adjusted the swath width showed the tradeoff between data accuracy and survey effort. A coverage rate of 3%–5% was suggested for surveys in environments like the lakes and rivers tested. The vessel was found to have good line-following performance and minimal pitch/roll deviations with an endurance of up to 3 h in practice. The process of echosounder tuning was also reviewed with example data illustrating real-world sensitivity and data errors/noise that were experienced. Lastly, several modes of deploying small USVs were introduced, and the relative advantages of each approach were discussed. The findings in this paper may be helpful to practitioners to gain an understanding of the capabilities, limitations, and workflow of using USVs for bathymetric data collection in inland bodies of water. However, the results may not be applicable to USVs that are substantially different from the HyDrone (e.g., USVs that are deployed in coastal waters, involve other sensor technologies such as multi-beam echosounders, or have other unique designs, instrumentation, or software).

Future work may include further characterization of small USV performance in adverse conditions, including strong currents and waves, and characterization of amphibious USVs that are tailored for very shallow-water operation. Additional evaluation of USV-based instrumentation, such as multi-beam sonar, forward-looking or side-scan (imaging) sonar, sub-bottom profilers, and acoustic Doppler current profilers, would also be beneficial for transportation agencies to understand the benefits and challenges of how such technologies can be used to assess bridge health and provide data to support hydraulic and hydrologic modeling. Lastly, enhancing the capabilities of USVs through advanced autonomy and perception algorithms may enable more robust operation, including risk-aware coverage path planning, GNSS-denied or GNSS-degraded navigation near bridges, and autonomous behaviors that detect and avoid hazards (e.g., vegetation, debris, and shallow water).

Article information

History dates

Received: 8 October 2025
Accepted: 10 February 2026
Accepted manuscript online: 14 February 2026
Version of record online: 17 March 2026

Copyright

© 2026 The Authors. This work is licensed under a Creative Commons Attribution 4.0 International License (CC BY 4.0), which permits unrestricted use, distribution, and reproduction in any medium, provided the original author(s) and source are credited.

Data availability

This manuscript does not report data.

Author information

Author ORCIDs

Alex Nikonowicz https://orcid.org/0000-0003-4934-5184

Author contributions

Conceptualization: AW
Funding acquisition: AW
Investigation: AN, AW
Methodology: AN, AW
Supervision: AW
Visualization: AN, AW
Writing – original draft: AN
Writing – review & editing: AN, AW

Competing interests

The authors declare no competing interests.

Funding information

This work was sponsored by the North Carolina Department of Transportation under award number 2024-20.

References

Adediran, E., Kastrisios, C., Lowell, K., Rice, G., and Zhang, Q. 2025. Toward quantifying interpolation uncertainty in set-line spacing hydrographic surveys. ISPRS Int. J. Geo-Inf. **14**(2): 90. doi:10.3390/IJGI14020090.

Allen, T.R., Eulie, D., Polk, M., Stuart, R., and Garnand, A. 2023. Advancing estuarine shoreline change analysis using small uncrewed

Drone Syst. Appl. Downloaded from cdnsciencepub.com by UNIV OF NC - CHARLOTTE on 03/18/26

autonomous systems. *In* Estuary Research: Recent Advances, IntechOpen. *Edited by* A.J. Manning. pp. 1–29. doi:10.5772/INTECHOPEN.112022.

Arseni, M., Voiculescu, M., Georgescu, L.P., Iticescu, C., and Rosu, A. 2019. Testing different interpolation methods based on single-beam echosounder river surveying. Case study: Siret River. ISPRS Int. J. Geo-Inf. **8**(11): 507. doi:10.3390/IJGI8110507.

Carilli, J.E., Guazzo, R.A., and Rodriguez, A.R. 2024. Applying an uncrewed surface vessel to measure under-pier bathymetry. IEEE J. Oceanic Eng. **49**(3): 793–801. doi:10.1109/JOE.2024.3360515.

Davenport, E., Nguyen, K., Jang, J., Ma, C., Fish, S., Lenain, L., and Meyer, F. 2025. A landmark-aided navigation approach using side-scan sonar. IEEE J. Oceanic Eng. **50**(4): 2672–2686. doi:10.1109/JOE.2025.3578230.

Johnson, A., Martin, P., Burkhalter, C., and Lutes, K. 2016. New remote sensing systems for improved planning and management of mine tailings storage facilities. *In* Proceedings of the 20th International Conference on Tailings and Mine Waste. pp. 891–903. Available from https://tailingsandminewaste.com/2016/TMW2016_Proceedings.pdf [accessed 28 November 2025].

Katsouras, G., Dimitriou, E., Karavoltsos, S., Samios, S., Sakellari, A., Mentzafou, A., et al. 2024. Use of unmanned surface vehicles (USVs) in water chemistry studies. Sensors, **24**(9): 2809. doi:10.3390/S24092809. PMID: 38732916.

Kumar, D., Ghorbanpour, A., Yen, K., and Soltani, I. 2025. Design and implementation of a dual uncrewed surface vessel platform for bathymetry research under high-flow conditions. IEEE Access, **13**: 106634–106651. doi:10.1109/ACCESS.2025.3580343.

Lee, K.H., Ali, S., Kim, Y., Lee, K., Kwon, S.Y., and Kam, J. 2023. High resolution mapping of nitrate loads of a reservoir using an uncrewed surface vehicle: potential opportunities and challenges. Water Resour. Res. **59**(11): e2023WR034665. doi:10.1029/2023WR034665.

Li, D., Shangguan, D., Wang, X., Ding, Y., Su, P., Liu, R., and Wang, M. 2021. Expansion and hazard risk assessment of glacial lake Jialong Co in the central Himalayas by using an unmanned surface vessel and remote sensing. Sci. Total Env. **784**: 147249. doi:10.1016/J.SCITOTENV.2021.147249.

Mach, B., and Skrzypek, M. 2022. Bathymetric measurements of a retention reservoir using integrated hydrographic and photogrammetric techniques. Comm.-Sci. Lett. Univ. Zilina, **24**(1): E19–E27. doi:10.26552/COM.C.2022.1.E19-E27.

Makar, A. 2022. Determination of the minimum safe distance between a USV and a hydro-engineering structure in a restricted water region sounding. Energies, **15**(7): 2441. doi:10.3390/EN15072441.

Marchel, L., Specht, C., and Specht, M. 2020. Assessment of the steering precision of a hydrographic USV along sounding profiles using a high-precision GNSS RTK receiver supported autopilot. Energies, **13**(21): 5637. doi:10.3390/EN13215637.

Ng, Y.H., Hou, Y., Yuan, Y., and Chang, C.W. 2024. Underactuated unmanned surface vessel coverage path planning for marine pier inspection. *In* Proceedings of MTS/IEEE OCEANS 2024 Conference and Exposition. pp. 1–10. doi:10.1109/OCEANS51537.2024.10682302.

Patterson, R.G., Lawson, E., Udyawer, V., Brassington, G.B., Groom, R.A., and Campbell, H.A. 2022. Uncrewed surface vessel technological diffusion depends on cross-sectoral investment in open-ocean archetypes: a systematic review of USV applications and drivers. Front. Marine Sci. **8**: 736984. doi:10.3389/FMARS.2021.736984.

Sardemann, H., Blaskow, R., and Maas, H. G. 2023. Camera-aided orientation of mobile LiDAR point clouds acquired from an uncrewed water vehicle. Sensors, **23**(13): 6009. doi:10.3390/S23136009. PMID: 37447858.

Schroeder, B., Haug, P., Alvarado, A., and Baribeau, S. 2019. Unmanned surface vessels for bridge scour monitoring (No. SPR-1682). Michigan Department of Transportation. Research Administration. pp. 1–100. Available from https://rosap.ntl.bts.gov/view/dot/66339 [accessed 28 November 2025].

Seafloor Systems, Inc. 2025. HyDrone. Available from https://www.seafloorsystems.com/hydrone [accessed 23 August 2025].

Specht, M., Specht, C., Lasota, H., and Cywiński, P. 2019. Assessment of the steering precision of a hydrographic Unmanned Surface Vessel (USV) along sounding profiles using a low-cost multi-Global Navigation Satellite System (GNSS) receiver supported autopilot. Sensors, **19**(18): 3939. doi:10.3390/S19183939. PMID: 31547372.

Specht, M., Specht, C., Szafran, M., Makar, A., Dąbrowski, P., Lasota, H., and Cywiński, P. 2020. The use of USV to develop navigational and bathymetric charts of yacht ports on the example of National Sailing Centre in Gdańsk. Remote Sens. **12**(16): 2585. doi:10.3390/RS12162585.

Drone Syst. Appl. Downloaded from cdnsciencepub.com by UNIV OF NC - CHARLOTTE on 03/18/26